analytical chemistry

Article

pubs.acs.org/ac

Direct Measurement of Resonance Raman Spectra and Cross Sections by a Polarization Difference Technique

Eric C. Le Ru,* Lina C. Schroeter, and Pablo G. Etchegoin*

The MacDiarmid Institute for Advanced Materials and Nanotechnology, School of Chemical and Physical Sciences, Victoria University of Wellington, P.O. Box 600, Wellington 6140, New Zealand

Supporting Information

ABSTRACT: Resonant Raman (RR) spectroscopy, despite its many promising applications in analytical chemistry and biology, remains an experimental challenge (compared to standard Raman) primarily because of the presence of large fluorescence backgrounds overwhelming the RR signals. The observation of RR spectra of fluorophores therefore requires the use of specialized, picosecond-time-resolved setups. Here, we present and demonstrate a method, based on polarization-difference, by which RR spectra and cross sections can be measured using the most standard Raman setup with continuous wave excitation and CCD-based detection. The method is applied to the dyes Nile Blue and rhodamine 6G under resonant excitation. This work should open a new era in RR spectroscopy, where RR spectra can be routinely measured and studied with conventional Raman systems.

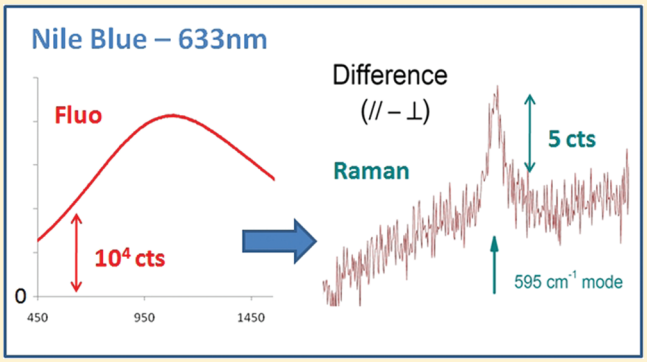

Since its discovery in 1928,[1] the applications of Raman spectroscopy have grown steadily, thanks primarily to instrumental advances (in particular the advent of lasers and CCD detectors). One remaining intrinsic hurdle is the fact that Raman signals are weak, typically ~12−14 orders of magnitude weaker than fluorescence, for example. Surface-enhanced Raman spectroscopy[2] endows a viable route to overcome this problem but introduces new experimental difficulties. A more direct solution comes from resonance Raman (RR) scattering,[3,4] where excitation in resonance with a molecular electronic absorption can boost the Raman signal by as much as ~4−5 orders of magnitude. This is particularly applicable to biologically relevant molecules[5−8] and can be further used as a powerful probe of excited states properties.[9−12] However, a well-known issue with RR is the concomitant large fluorescence background intrinsically linked to the molecule we wish to detect. Extrinsic fluorescence is also present in a much wider context, especially in biological environments such as cells. This problem is as old as the technique itself and has led to the well established dogma that RR spectra of fluorophores cannot be obtained under standard conditions. Fluorophores with extremely low fluorescence quantum yields (QY ~ 10^{-5}–10^{-3}) constitute an exception[12,13] with important applications in biology.[5] Fluorescence may also be quenched by other means,[14,15] although this typically affects other molecular properties. Fluorescence background suppression methods have therefore been developed: polarization modulation and lock-in techniques,[16,17] shifted-excitation difference Raman spectroscopy (SERDS),[18] wavelength-modulation,[19] and phase-modulation.[20] These methods allow the study of fluorophores with poor QYs, up to typically 0.1−1% but remain far from the RR requirements for dyes with moderate or good QYs. They also require modifications to standard Raman setups. Only time-resolved techniques,[6−8,11,21−23] which exploit the fact that Raman is instantaneous while fluorescence is delayed (by ≈1 ps−10 ns), have so far been able to measure RR spectra of the most efficient fluorophores but with a dramatic increase in experimental complexity. Still, such methods are not well suited for dyes with moderate QYs of ~1−10%, because of the shorter fluorescence lifetimes. They also have additional limitations in terms of the achievable spectral resolution (much larger than typical Raman peaks).[21,23] Moreover, such experiments remain challenging; for example, the first measurement of RR cross sections for Rhodamine 6G (RH6G) (one of the most widely used fluorescent dyes in the history of laser spectroscopy) dates only from 2008, when they were measured for a single excitation wavelength (532 nm) using broadband stimulated femtosecond time-resolved Raman spectroscopy.[23] The experimental complexity of such methods makes them inadequate to routine applications.

In this work, we show that polarization-difference techniques can overcome the problem of fluorescence backgrounds with the most standard Raman setup based on continuous wave (CW) excitation and CCD detection. This is accomplished by careful subtraction of two polarized Raman spectra, to remove the so-called fixed-structure noise contribution to the signal. Hence, we call the method polarization-difference resonance

Received: March 18, 2012
Accepted: May 3, 2012
Published: May 3, 2012

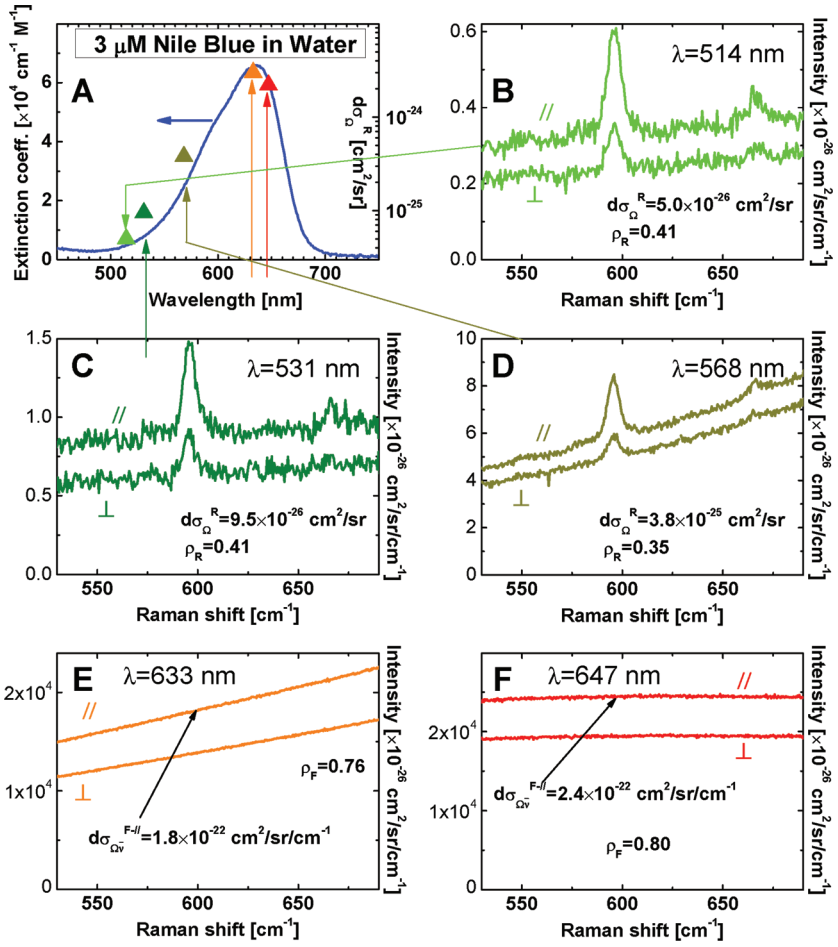

Figure 1. Fluorescence/Raman signals in the approach to resonance for NB in water. (A) Absorption spectrum, together with the Raman excitation profile for five laser lines (symbols), as determined in this work. (B–D) Raman spectra (3 μM) for both polarization configurations (∥ and ⊥) around the region of the 595 cm^{-1} fingerprint mode of NB at excitation wavelengths approaching resonance (514, 531, and 568 nm, respectively). From the latter, the Raman cross sections $d\sigma_\Omega{}^R$ and depolarization ratio, ρ_R, can be directly obtained. ρ_R approaches its expected resonance value of 1/3 close to resonance (568 nm). (E,F) Fluorescence spectra (0.5 μM) in RR conditions at 633 and 647 nm. The fluorescence background increases by ∼10^3, and the Raman peaks are no longer visible. Still, the fluorescence cross-section $d\sigma^F_{\Omega\bar{\nu}}$ and depolarization ratio ρ_F at 595 cm^{-1} can be measured and will be used to normalize the RR intensities in the PD-RRS spectra.

Raman spectroscopy (PD-RRS). The resulting noise in the PD-RRS spectrum is shown to be shot-noise (photon) limited and can therefore be reduced to as low as 10^{-4}–10^{-5} (noise-to-background ratio) with long acquisitions. The method is demonstrated by measuring the RR cross sections and excitation profile of the 595 cm^{-1} mode of Nile Blue (NB) in water, whose moderate QY (≈4%) makes it difficult to study with other methods. We also apply it to NB in ethanol (QY 25%) and rhodamine 6G in water (QY 95%), demonstrating its wide range of applicability (up to the best fluorophores). Additionally, RR peaks with full-width at half-maximum (fwhm) as small as 4 cm^{-1} are demonstrated; a resolution that would be impossible to measure with most time-resolved techniques. This work therefore solves a 50-year old problem in Raman spectroscopy, namely, the measurement of RR peaks of fluorescent dyes with CW excitation. This work should establish the routine use of RR spectroscopy as a powerful tool for applications in analytical chemistry and biological sciences. More generally, the method could be adapted to other CCD spectroscopic or imaging studies where an extremely small (but tunable in intensity) signal must be detected over a large fixed background.

EXPERIMENTAL RESULTS

Raman/fluorescence experiments were performed in the conventional 90°-scattering configuration for liquids (see Figure S1 in the Supporting Information), with fixed polarization in detection and a varying (parallel, ∥, or perpendicular, ⊥) incoming polarization selected by a $\lambda/2$ waveplate (see sections S.I and S.II of the Supporting Information for further details). Figure 1 presents the results of a standard CW Raman/fluorescence measurement at several excitation wavelengths for NB in water. RR spectra and cross sections can be measured in preresonance conditions and are in agreement with reported values.[9] However, despite the moderate QY (≈4%), the fluorescence background at resonance (633 and 647 nm) is so large that it prevents any direct observation of the Raman peak, whose intensity is (as we shall show) ≈5 × 10^{-4} smaller. This could, in principle, be overcome by increasing integration times (or total number of collected photons N) to reduce the relative noise (defined as rms noise over signal) to, say, $\varepsilon \approx 10^{-4}$. An important (and intrinsic) source of noise is photon noise (shot noise), for which $\varepsilon_{ph} = 1/\sqrt{N}$. We would therefore need $N \approx 10^8$ if shot-noise is the only contribution; and this is

dx.doi.org/10.1021/ac300763q | Anal. Chem. 2012, 84, 5074–5079

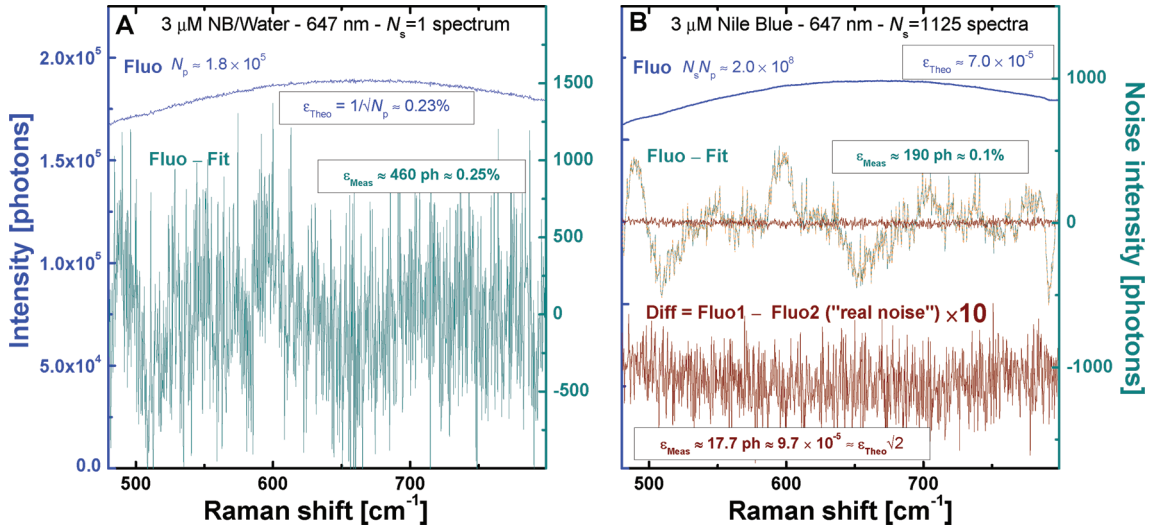

Figure 2. Photon and fixed-structure noise in CCD measurements of fluorescence. (A) Fluorescence obtained from N_s = 1 spectrum and residual after subtraction of a 4th-order polynomial fit to reveal the noise structure and amplitude (dominated by photon noise in this case). The measured relative rms noise ε_{Meas} is consistent with that predicted for photon noise with $N_p = 1.8 \times 10^5$ photons per CCD bin ($\sim 1/(N_p)^{1/2}$). (B) Average fluorescence obtained from N_s = 1125 spectra and residuals for two different series of 1125 spectra. The residuals are almost identical and are therefore dominated by fixed-structure noise. This noise can be removed by subtraction of two average fluorescence spectra (or their residuals), and we then recover the predicted photon noise (dark red), with no apparent spectral structure (as expected). The relative rms noise after subtraction is only $\varepsilon_{Meas} \sim 9.7 \times 10^{-5}$, consistent with its theoretical value of $(2/(N_s N_p))^{1/2}$.

easily achievable with modern CCDs (see sections S.III and S.IV of the Supporting Information).

However, another source of noise dominates in this range, and this is illustrated in Figure 2 (see also sections S.III and S.IV of the Supporting Information). The fluorescence spectrum (in a small energy window suitable for Raman) of NB excited at 647 nm was measured over N_s = 5000 consecutive spectra, with $N_p \approx 1.8 \times 10^5$ photons per wavelength on average in each spectra (adjusted to be just under the saturation limit of the linear dynamic range of our CCD). A representative spectrum is shown in Figure 2A, together with the noise analysis. In order to reveal the noise, a fourth-order polynomial fit is subtracted and the absolute rms noise is then obtained from the standard deviation of the residual (shown in Figure 2A). Here, the measured relative rms noise, ε_{Meas} is close to the expected value for photon noise, ε_{ph}. As we increase the number of collected photons ($N = N_s N_p$) by averaging more spectra (Figure 2B) and therefore decrease the relative photon noise; the residual noise does not decrease substantially. Instead, it exhibits increasingly well-defined features (shown in Figure 2B). This fixed-structure noise is also stable over time and can be consistently measured in a successive series of spectra. This is a well-known problem of CCD imaging in astronomy and is associated with nonuniformity in the CCD response (i.e., pixel-to-pixel variations in efficiency and/or linearity, imperfections in electronic read-out, etc.). It can typically be removed by careful measurements of the flat-field response. In the case of spectroscopy there are a number of additional contributions to CCD fixed-structure noise, including, for example, stray light or scattering from the optical elements. As a result, part of this fixed-structure noise will depend on the exact experimental configuration, including grating position, collecting optics alignment, etc., and because of these, flat-field corrections cannot efficiently eliminate it. Image subtraction (applied to spectra here) does, however, provide an efficient way of eliminating fixed-structure noise. For perfect cancellation, this should result in a residual noise of $\varepsilon\sqrt{2}$, where ε is the stochastic rms noise (excluding fixed structure noise) of the two original spectra. This subtraction is illustrated in Figure 2B, and the relative noise in the residual spectrum is 9.7×10^{-5} and equal within experimental errors to the best allowed by the intrinsic shot-noise in the two original spectra (each with $\varepsilon_{ph} \approx 7 \times 10^{-5}$). In fact, this method can be used to "measure" the number of photons contained in the spectra, and it demonstrates that photon-noise limited spectra are attainable. Notwithstanding, in the straightforward implementation of Figure 2B we also lose all useful signal in the subtraction. In order to apply the method to an actual signal measurement (rather than just a noise study), it is necessary to change the signal intensity while retaining the fixed-structure noise magnitude and spectral shape. In the context of RR, this can be done by using the polarization properties of the Raman emission. With polarized detection, one can modulate the RR signal simply by changing the incident polarization. This can be achieved with minimal changes in the optical setup and, with sufficient care, with no change in the fixed-structure noise.

The main steps in the practical implementation of PD-RRS are illustrated in Figure 3, for the case of NB in water excited at 647 nm (other examples are provided in section S.VIII of the Supporting Information). N_s = 2500 spectra were obtained for each polarization. The integration time for ∥-polarization was first adjusted to obtain spectra close in intensity to the maximum linear dynamic range of our CCD (used in the low-gain mode to collect as many photons as possible per spectra). Because of slight nonlinearities in the fixed-structure noise, it is necessary for the method to work at its best to obtain ⊥-polarization spectra with the same intensity as the ∥ one (within a few %). Because the fluorescence depolarization is not exactly one ($\rho_F \approx 0.8$ in our example), we therefore also adjust the integration time for the ⊥-polarization. Using the CCD in fast mode, spectra can be acquired with a small delay (less than 0.1 s) between spectra, giving a total measurement time of 20 min for 2500 spectra (and about 10 min for data processing/transfer in our system). Hence, the whole experiment takes

dx.doi.org/10.1021/ac300763q | Anal. Chem. 2012, 84, 5074−5079

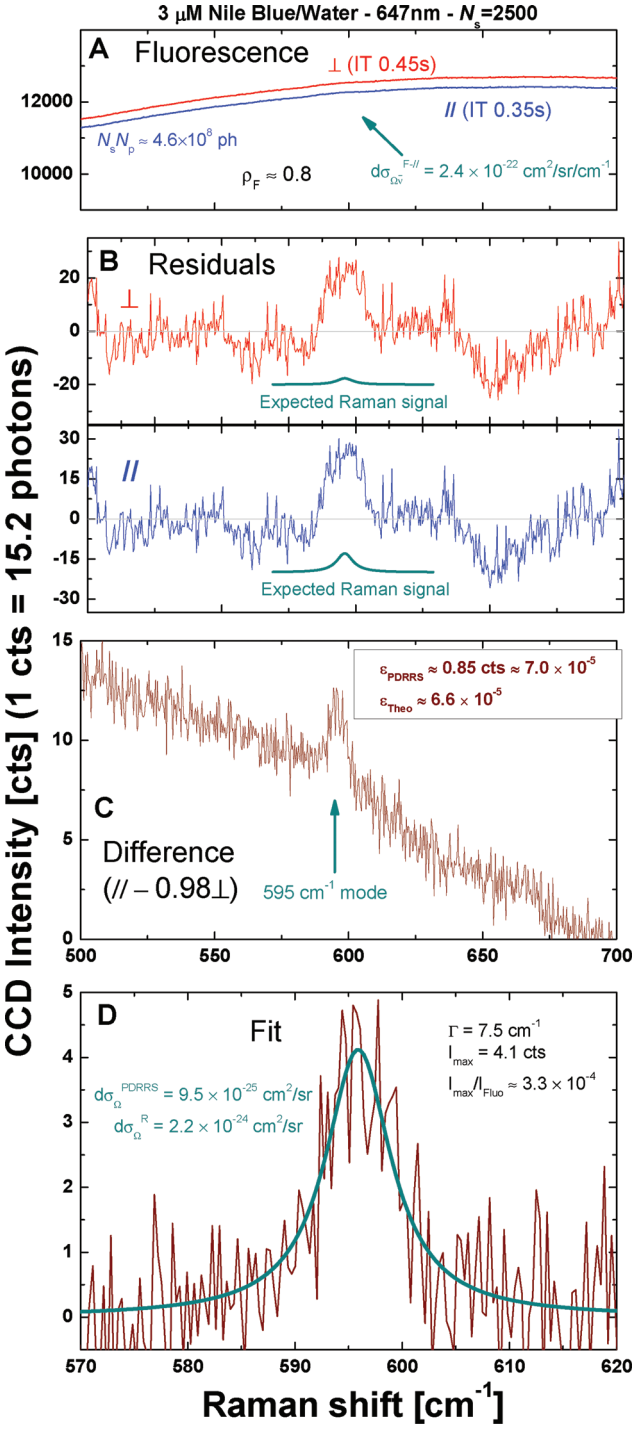

Figure 3. Example of PD-RRS measurement: 595 cm^{-1} mode of NB at 647 nm excitation, using N_s = 2500 spectra for each polarization. (A) Fluorescence spectra for each polarization. Note the different integration time (IT) to account for the fluorescence depolarization ratio $\rho_F \approx 0.8$. (B) Residuals of part A after 4th-order polynomial subtraction, showing an almost identical fixed-structure noise. The predicted intensities of the Raman peaks (computed *a posteriori*) are indicated as a guide. (C) PD-RRS spectrum obtained from subtraction of the ∥ and ⊥ configuration average spectra, where the Raman peak is clearly visible. (D) PD-RRS spectrum in the Raman peak region and Lorentzian fit to the peak. The corresponding cross-section is inferred with respect to the fluorescence intensity background (from an independent measurement of the fluorescence cross-section). Further examples are given in section S.VIII of the Supporting Information.

about an hour, from which we only need to extract the average spectra for each polarization as shown in Figure 3A. For the method to work, the fixed-structure noise (evidenced earlier in Figure 2) must be identical for each polarization. This can be inspected directly by subtraction of a fourth-order polynomial to the fluorescence spectra, as shown in Figure 3B. It is interesting to note that the expected Raman peak (obtained at the end but shown for comparison here) is entirely buried in the fixed-structure noise. This is the reason why plain integration for a single polarization as in Figure 1F can never resolve the RR signal. Nevertheless, the difference of both spectra reveals the remaining shot-noise limited signal, as shown in Figure 3C where the 595 cm^{-1} peak of NB under resonant excitation can be clearly seen. The remaining noise in this spectrum agrees (excluding the Raman peak region and within experimental uncertainty) with expectations for the relative photon-noise: $\varepsilon_{PDRRS} \approx 7 \times 10^{-5}$ (i.e., $\sqrt{2}$ times the photon noise of the original average fluorescence spectra).

RESONANCE RAMAN CROSS-SECTION

Finally, the obtained PD-RRS spectra can be used to extract the RR cross sections, as illustrated in Figure 3D. The resulting peak is fitted to a Lorentzian with a linear background. The relatively high dispersion used in this experiment (wavenumber spacing between consecutive pixels = 0.34 cm^{-1}) results in a large number of data points and improves the fit reliability. We also note the presence of small Fabry–Perot oscillations, which are associated with glass interfaces in the collecting optics. These are normally invisible but become apparent when resolving fine details at a level of ~10^{-4} relative signal, and they do not disappear completely during subtraction because of a slight polarization dependence. It is interesting to point out also that the obtained full-width at half-maximum (fwhm), Γ, is much narrower than what is typically achievable with time-resolved RR methods. To relate the observed peak intensity to an absolute differential Raman cross-section $d\sigma_\Omega^{PDRRS}$, we use the fluorescence intensity for ∥-polarization as a reference (see sections S.V and S.VI of the Supporting Information), which we measured independently to be $d\sigma_{\Omega\nu}^{F-\parallel} = 2.4 \times 10^{-22}$ $cm^2/sr/cm^{-1}$ in this case. The latter measurement is carried out at low laser power density and low dye concentration. This two-step determination of the absolute cross-section is self-normalizing with respect to photobleaching and reabsorption (of laser or Raman light) in the cell. The final step is to determine the absolute RR cross-section $d\sigma_\Omega^R$ from the measured one $d\sigma_\Omega^{PDRRS}$ (difference between ∥- and ⊥-polarization, the latter with $1/\rho_F$ longer integration time) from the relation:

$$d\sigma_\Omega^R = \frac{1+\rho_R}{1-\rho_R/\rho_F} d\sigma_\Omega^{PDRRS} \quad (1)$$

where ρ_R is the Raman, and ρ_F is the fluorescence depolarization ratios, respectively. In most instances, ρ_R can be easily predicted in RR conditions,[3] since the RR peak intensities are dominated by the intermediate electronic dipole-allowed transition in the Raman process. For example, for the common case of a single nondegenerate electronic transition ρ_R = 1/3. In the case of NB, we can even confirm experimentally that ρ_R indeed approaches 1/3 for the 595 cm^{-1} at 568 nm (preresonance condition), where a standard Raman measurement can still be performed (see Figure 1).

In the example of Figure 3, we obtained $d\sigma_\Omega^R = 2.2 \times 10^{-24}$ cm^2/sr, similar to known RR cross-sections of other dyes at

dx.doi.org/10.1021/ac300763q | Anal. Chem. 2012, 84, 5074–5079

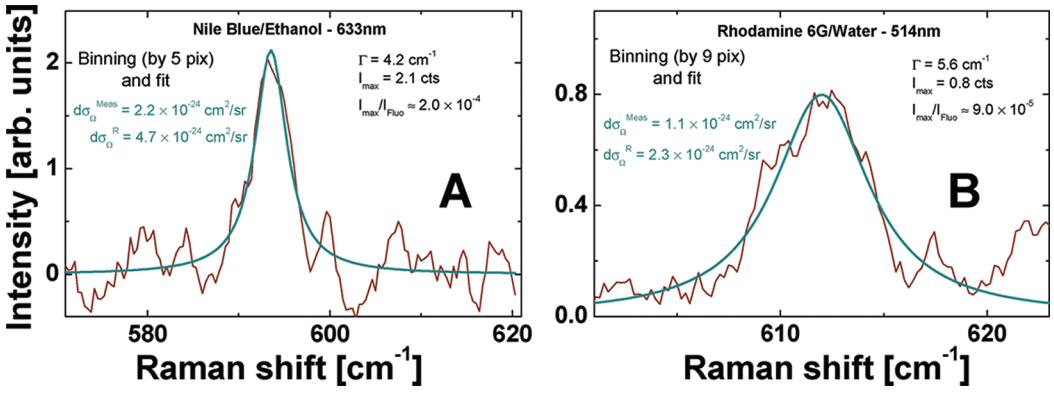

Figure 4. RR cross sections of good fluorophores from PD-RRS: (A) 595 cm^{-1} mode of NB in ethanol (QY ≈ 25%) at 633 nm excitation, using N_s = 7000 spectra for each polarization. (B) 612 cm^{-1} mode of rhodamine 6G in water (QY ≈ 95%) at 514.5 nm excitation, using N_s = 20 000 spectra for each polarization. In both cases, binning is carried out along the spectral direction to further improve the relative noise. This can be done while preserving a good spectral resolution thanks to the high dispersion.

resonance.[23] We re-emphasize the dramatic nature of this result: in order to obtain it, we had to extract a shot-noise limited Raman signal with a relative peak intensity with respect to the fluorescence background of only 3.3×10^{-4} (Figure 3). The same measurement was also carried out at 633 nm (Figure S8 of Supporting Information) to complete the RR excitation profile of NB in water shown earlier in Figure 1A.

DISCUSSION AND CONCLUSIONS

The PD-RRS method as presented here is fairly general and can be applied to any excitation wavelength and other dyes with moderate to good quantum yields. The main requirement is that the fluorescence signal is more depolarized than the Raman peaks, a condition that is satisfied in most common cases (an example of a case where it might sometimes fail is that of a fluorophore in a high-viscosity solvent). Although the method was demonstrated here using a 90°-scattering configuration for liquids and a triple Raman spectrometer, it can readily be extended to other Raman setups and to solid samples. We have, for example, also obtained (not shown here) the PD-RRS spectrum of Nile Blue at 633 nm using a Jobin-Yvon Labram Raman microscope, which uses the backscattering configuration with a notch filter and a single spectrometer.

To further illustrate the power of the PD-RRS, we have also measured the RR cross-section of the 594 cm^{-1} mode of NB in ethanol (with a larger fluorescence QY of 25%) and of the 612 cm^{-1} mode of Rhodamine 6G at 514 nm (QY of 95%), as shown in Figure 4 (see also Figures S6 and S7 and Tab. S.I in the Supporting Information). The latter is considered as the most difficult case of RR and has so far only been studied using the most advanced time-resolved methods and only at 532 nm excitation.[21,23] The RR cross-section determined from PD-RRS, which can be implemented in any standard Raman spectrometer, is in good agreement with such measurements.[23] It is worth highlighting again the narrow linewidths measured with PD-RRS (down to ∼4 cm^{-1} fwhm only), which are inaccessible in time-resolved techniques with typical spectral resolution of the order of 20 cm^{-1}. We envisage that the simplicity of implementation, power, and general applicability of this method should herald a new era in Raman spectroscopy, where RR spectra can be routinely acquired with the best spectral resolution and RR cross sections can be easily measured. This work indeed explicitly demonstrates, against the dogmas of Raman spectroscopy, that resonant Raman spectra of fluorescent dyes can be directly obtained with CW excitation and conventional Raman systems.

ASSOCIATED CONTENT

Supporting Information

Further experimental details, detailed description of the noise sources and of their experimental characterization, and further experimental results of PD-RRS measurements of Nile Blue and Rhodamine 6G. This material is available free of charge via the Internet at http://pubs.acs.org.

AUTHOR INFORMATION

Corresponding Author

*E-mail: eric.leru@vuw.ac.nz (E.C.L.R.); pablo.etchegoin@vuw.ac.nz (P.G.E.).

Notes

The authors declare no competing financial interest.

ACKNOWLEDGMENTS

E.C.L.R. is indebted to the Royal Society of New Zealand (RSNZ) for support through a Marsden Grant and Rutherford Discovery Fellowship. P.G.E. acknowledges support from a Marsden Grant of the RSNZ.

REFERENCES

(1) Raman, C. V.; Krishnan, K. S. *Nature* **1928**, *121*, 501−502.
(2) Le Ru, E. C.; Etchegoin, P. G. *Principles of Surface Enhanced Raman Spectroscopy and Related Plasmonic Effects*; Elsevier: Amsterdam, The Netherlands, 2009.
(3) Clark, R. J. H.; Dines, T. J. *Angew. Chem., Int. Ed.* **1986**, *25*, 131−158.
(4) Efremov, E. V.; Ariese, F.; Gooijer, C. *Anal. Chim. Acta* **2008**, *606*, 119−134.
(5) Spiro, T. G.; Strekas, T. C. *Proc. Natl. Acad. Sci.* **1972**, *69*, 2622−2626.
(6) Benniston, A. C.; Matousek, P.; McCulloch, I. E.; Parker, A. W.; Towrie, M. *J. Phys. Chem. A* **2003**, *107*, 4347−4353.
(7) Kukura, P.; McCamant, D. W.; Yoon, S.; Wandschneider, D. B.; Mathies, R. A. *Science* **2005**, *310*, 1006−1009.
(8) Fang, C.; Frontiera, R. R.; Tran, R.; Mathies, R. A. *Nature* **2009**, *462*, 200−204.
(9) Lawless, M. K.; Mathies, R. A. *J. Chem. Phys.* **1992**, *96*, 8037−8045.
(10) Myers, A. B. *Acc. Chem. Res.* **1997**, *30*, 519−527.

(11) Kwok, W. M.; Ma, C.; Matousek, P.; Parker, A. W.; Phillips, D.; Toner, W. T.; Towrie, M.; Umapathy, S. *J. Phys. Chem. A* **2001**, *105*, 984−990.
(12) Stuart, C. M.; Frontiera, R. R.; Mathies, R. A. *J. Phys. Chem. A* **2007**, *111*, 12072−12080.
(13) Galloway, C. M.; Etchegoin, P. G.; Le Ru, E. C. *Phys. Rev. Lett.* **2009**, *103*, 063003.
(14) Xie, L.; Ling, X.; Fang, Y.; Zhang, J.; Liu, Z. *J. Am. Chem. Soc.* **2009**, *131*, 9890−9891.
(15) Meyer, S. A.; Le Ru, E. C.; Etchegoin, P. G. *J. Phys. Chem. A* **2010**, *114*, 5515−5519.
(16) Arguello, C. A.; F., M. G.; Leite, R. C. C. *Appl. Opt.* **1974**, *13*, 1731−1732.
(17) Angel, S. M.; DeArmond, M. K.; Hanck, K. W.; Wertz, D. W. *Anal. Chem.* **1984**, *56*, 3000−3001.
(18) Shreve, A. P.; Cherepy, N. J.; Mathies, R. A. *Appl. Spectrosc.* **1992**, *46*, 707−711.
(19) De Luca, A. C.; Mazilu, M.; Riches, A.; Herrington, C. S.; Dholakia, K. *Anal. Chem.* **2010**, *82*, 738−745.
(20) Genack, A. Z. *Anal. Chem.* **1984**, *56*, 2957−2960.
(21) Matousek, P.; Towrie, M.; Parker, A. W. *J. Raman Spectrosc.* **2002**, *33*, 238−242.
(22) Wilbrandt, R. *Biospectroscopy* **1996**, *2*, 263−275.
(23) Shim, S.; Stuart, C. M.; Mathies, R. A. *ChemPhysChem* **2008**, *9*, 697−699.

Supporting information for "Direct measurement of resonance Raman spectra and cross-sections by a polarization difference technique"

Eric C. Le Ru,* Lina Schröter, and Pablo G. Etchegoin†

The MacDiarmid Institute for Advanced Materials and Nanotechnology, School of Chemical and Physical Sciences, Victoria University of Wellington, PO Box 600, Wellington 6140, New Zealand

Contents

S.I. SAMPLE PREPARATION

Rhodamine 6G (R6G) (dye content 95%) and Nile Blue A perchlorate (NB, dye content 95%) were purchased from Sigma-Aldrich. Extra precautions must be taken because of the poor solubility of NB in water, and its tendency to form aggregates. For example, inconsistent results were obtained when preparing samples from a 100 μM NB/water solution. A 2 L stock solution of NB in water was therefore prepared at a relatively low concentration of 12 μM and magnetically stirred for a week (it takes a few days for NB to fully dissolve properly, as corroborated by absorption measurements). Other samples were then prepared by further dilution from this stock reference solution. The absorbance then scales linearly with concentration below 6 μM. As shown in Fig. S1, a small shoulder is still evident at 12 μM, suggesting the onset of the creation of dye-aggregates (probably dimers) at this concentration. Only solutions of NB/water at concentrations of 6 μM and below were therefore used in the measurements. The NB/ethanol solutions were also prepared from a 2 L stock solution at 12 μM concentration.

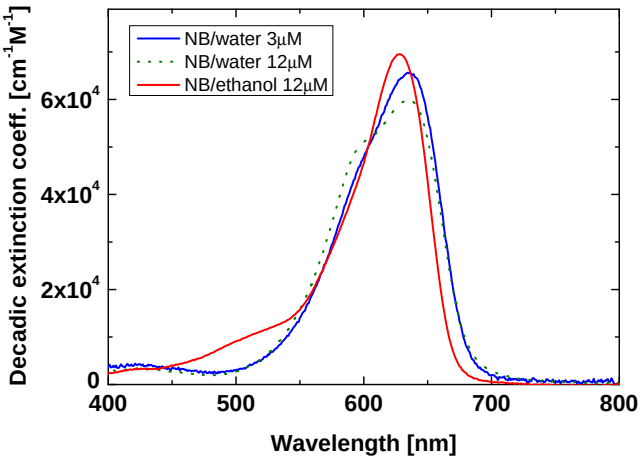

FIG. S1: UV-Vis absorption of NB in water and ethanol. The change in the spectrum of NB/water from 3 μM to 12 μM suggests the onset of dye-aggregation around $\sim$ 10 μM. The spectrum in ethanol is modified by solvation effects.

There was no evidence of solubility or dye-aggregation issues in this case. The absorbance spectrum is slightly modified in ethanol by solvation effects (see Fig. S1); its maximum position is in particular blue-shifted to 628 nm (down from 634 nm in water).

*Electronic address: eric.leru@vuw.ac.nz
†Electronic address: pablo.etchegoin@vuw.ac.nz

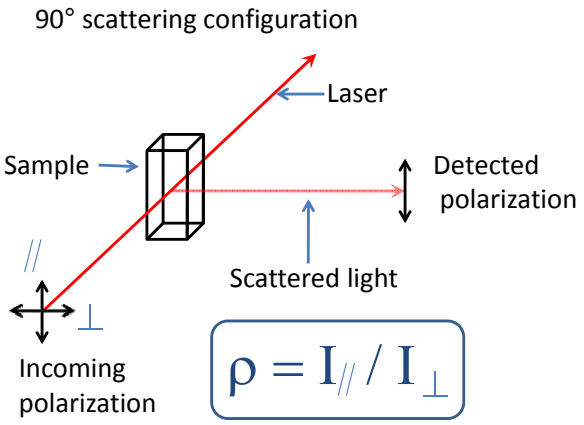

FIG. S2: Basic 90°-scattering configuration. The detection is always performed in the (fixed) vertical direction to avoid differences in instrumental efficiencies. The excitation is either $\parallel$ or $\perp$ to the detection direction (selected by an achromatic $\lambda/2$ waveplate), and is focused in the center of the cell by a $f = 15\,\mathrm{cm}$ focal length lens (not shown). The collection of the signal is done by two lenses of focal length $f = 10\,\mathrm{cm}$ each, thus achieving an image of magnification=1 on the entrance slit ($300\,\mu\mathrm{m}$) of the monochromator (T64000 Jobin-Yvon triple additive/subtractive spectrometer coupled to a lquid-nitrogen-cooled Symphony CCD with fast acquisition mode). The depolarization ratio (for either Raman or fluorescence) is defined as the ratio of intensities: $\rho = I_\perp / I_\parallel$.

S.II. FURTHER DETAILS ON THE EXPERIMENTAL SET-UP

The basic experimental set-up is presented in Fig. S2. For PD-RRS to work well, there is a number of experimental aspects that require special attention, in order to make sure that the acquired fluorescence spectrum and associated fixed-structure noise are identical for both polarizations. For this, it is important to take the following precautions:

- The polarizing optics (to change the incident polarization) should not introduce any change in the incident beam path (this affects both stray light and collected light path, and result in changes in the fixed structure noise). This can be achieved by a careful optical alignment. It is also beneficial to have a small magnification in the collecting optics between sample and entrance slit (we used $\times 1$ in our experiments) to minimize the effect of any remaining imperfections.

- Any Fabry-Perot (FP) interferences at any point in the collecting path have a small polarization dependence, which can become problematic in the PD-RRS spectrum, especially for the lowest relative noise levels of $\epsilon \sim 10^{-4}$ and below. One should bear in mind that by the time the data has been reduced to this level, we are looking at really small amplitude components in the signal that would never be evident or easily observable in the raw data. All the optical components that follow the light trail from the laser beam inside the cell to the CCD detector are obviously transparent to visible light. But the small reflectivities that can arise by the index mismatches of the glass components with air are enough to sometimes contribute to Fabry-Perot-like interferences (typically associated with 0.1–5 mm glass windows) in the reduced spectrum. An example of how bad the problem can be is shown for illustration in Fig. S3. In such an extreme situation, Fourier filtering can be used to clean-up the spectrum, but this does not work well in general (for example, when there is a background that is not flat, or when multiple FP interferences result in complex patterns). It is therefore important to minimize these FP interferences experimentally as much as possible. For example, we use a thick ($\sim 2\,\mathrm{cm}$) Glan-Thompson polarizer in collection instead of a sheet polarizing filter (which was used in the example of Fig. S3 to show the effect of FP interferences). Moreover, we further reduced FP-like patterns by using a thick glass cube ($\sim 1\,\mathrm{cm}$) attached to the glass cell on the face from which the light is collected. The cube is stuck to the window cell with optical oil (the same used in oil immersion objectives) and it achieves an effective window on the collection side of the cell that is much thicker than the standard one. This reduces small FP interferences by a great amount. We also turn slightly the cell at an angle ($\sim 5°$), to help further wash out FP interferences in the collected signal.

S.III. NOISE SOURCES IN CCD MEASUREMENTS

The amplitude of noise in a given spectrum can be characterized by ϵ, the root-mean-square (rms) of the spectrum after subtraction of the real signal (fluorescence and/or Raman). ϵ can be expressed as absolute noise in counts (cts) or photons, or normalized with respect to the intensity of the spectrum (also in counts or photons) to obtain the relative noise (i.e. noise-to-signal ratio) as quoted for example in Figs. 2 and 3 of the main text. The most common sources of noise in a CCD measurement and their dependence on parameters such as the number of collected photons (per wavelength or CCD bin) are well-understood. In PD-RRS experiments, the number of collected photons per bin for a single spectrum, N_p, is large and is mainly limited by the dynamic range of the CCD ($N_p \approx 1.8 \times 10^5$ photons in our system, using the CCD in its lowest gain mode of 15.2 photons/cts). It is therefore necessary to average over a number of spectra, N_s, to further increase the total number collected photons $N = N_s N_p$. The dependence of the most important

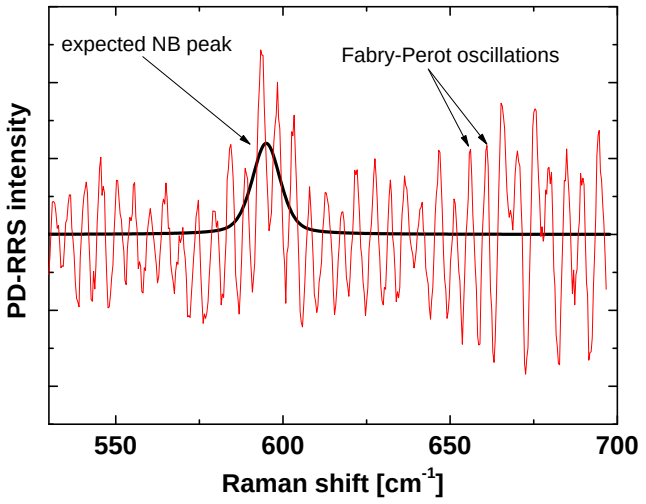

FIG. S3: PD-RRS of NB in water at 633 mn acquired using a sheet polarizing filter in collection, instead of a thick Glan-Thompson polarizer. The signal is clearly dominated by a Fabry-Perot interference pattern, with an amplitude of $\sim 10^{-3}$ with respect to the original (before subtraction) signal intensity. As a result, the Raman peak is hardly visible. Fabry-Perot interferences of the cell window or other dielectric optical components in the collection optics become an issue at this signal level, and they must be minimized by experimental means (like increasing the thickness of the cell window).

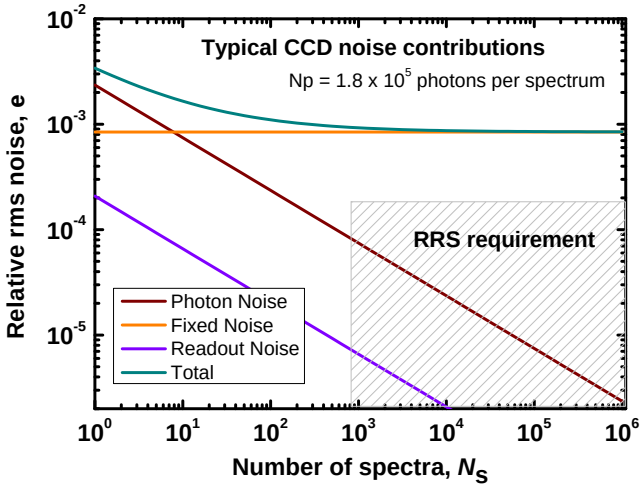

FIG. S4: Typical CCD noise contributions. The total relative rms noise (ϵ) is split into its contributions from: (i) photon noise, (ii) fixed noise, and (iii) readout noise. As a function of the number of spectra N_s, readout noise (purple) and photon noise (brown) scale like $1/\sqrt{N_s}$, while fixed (structure) noise (orange) is constant. The total noise (green) is the sum of all contributions, and is clearly dominated by the fixed structure noise for large N_s. The region that needs to be accessed for RR measurements is shown in the shaded area on the bottom right corner. The technique of PD-RRS eliminates the fixed noise contribution, and the photon-noise limited signal that contains the RR spectrum can be accessed.

sources of noise can then be predicted as follows.

- Photon-noise (shot-noise): This is an intrinsic property of light, and the relative noise can be deduced from the total number of collected photons as $\epsilon_{\rm Ph} = 1/\sqrt{N} = 1/\sqrt{N_s N_p}$. This noise is stochastic and spectrally white (i.e. it has no spectral structure or correlation).

- Read-out noise: This type of noise is typically linked to the electronic noise, associated with the read-out of the CCD array and is of the order of 1–2 electrons for a single read-out (about 25 photons in low gain mode, or 1.5×10^{-4} relative noise for $N_p = 1.8 \times 10^5$ ph). This noise is also stochastic and spectrally white with no spectral structures or correlation. It therefore scales as $\sqrt{N_s}$ for N_s spectra, and can therefore be reduced by acquiring more spectra. Its overall contribution to the relative noise in our case is $\epsilon_{\rm r-o} \approx 1.5 \times 10^{-4}/\sqrt{N_s}$ and is therefore negligible in all cases (it does however play an important role in low-signal-level detection with CCDs). .

- Fixed-structure noise: By definition this type of noise is the same in consecutive measurements and presents clear spectral features, as shown for example in Figs. 2B and 3B of the main text, and in the additional experimental data in Sec. VIII. In fact, because it is not stochastic in nature, one could argue that it should not be called noise at all, but we keep this denomination here as it represents an "unwanted" signal. It arises from systematic imperfections in the CCD array (pixel-to-pixel variations in efficiency, linearity, etc...) or in the electronic readout. In the case of spectroscopy, it also arises from spatial imperfections in the optical elements and/or stray light. In a first approximation, all these result in a linear dependence of the fixed-structure noise spectrum with the number of collected photons, and it cannot therefore be removed by longer integrations. The corresponding relative noise is constant (for a given experiment), and of the order of $\epsilon_{\rm Fix} \approx 0.1\%$ in the examples presented in this work.

Assuming large signal intensities, limited only by the dynamic range of the CCD ($N_p \approx 1.8 \times 10^5$), we have plotted the predicted dependence of each type of noise on the number of acquired spectra in Fig. S4. It is clear that the fixed-structure noise is the major obstacle to experiments where a small signal must be detected over a large background, as is the case for direct RR measurements. If this can be removed –as in PD-RRS– the photon-noise limited spectrum can be regained, and relative noise levels of 10^{-4} and below can be achieved by acquisition of $N_s \sim 10^3 - 10^4$ spectra (in our experimental conditions).

S.IV. NOISE MEASUREMENTS AND TESTS

In all measurements, the noise level ϵ was experimentally determined by computing the root-mean-square (rms) of the spectrum after subtraction of a fourth-order polynomial (obtained from a linear least square fit). ϵ can be expressed as absolute noise in counts (cts) or photons, or normalized with respect to the intensity of the spectrum (also in counts or photons) to obtain the relative noise (i.e. noise-to-signal ratio), as quoted for example in Figs. 2 and 3 of the main text. For a spectrum dominated by fluorescence, the 4th-order-polynomial-subtracted data provides essentially the noise spectrum, which (for most cases considered here) is strongly dominated by the fixed-structure noise. As explained in Fig. 2 of the main text, this can be removed by subtraction to study other sources of noise. In most PD-RRS spectra, the relative noise $\epsilon_{\mathrm{PDRRS}}$ is expressed as the residual rms noise in the PD-RRS spectrum (outside any regions where a Raman peak is present), normalized to the intensity of the original spectra (parallel or perpendicular polarization). If the fixed-structure noise is correctly removed in the difference spectrum, then $\epsilon_{\mathrm{PDRRS}} \approx \epsilon_{\mathrm{Ph}}\sqrt{2}$, where ϵ_{Ph} is the predicted photon noise in the original polarized spectra.

In all PD-RRS measurements, we have carried out systematic noise test to ensure that the acquired polarized spectra were photon-noise limited (after fixed-structure noise removal), and that this shot noise could be reduced by averaging over many spectra. Such a test is important to ensure that the experiments are not affected by other unknown sources of noise (and is a more detailed version of what is presented in the main text in Fig. 2). Basically, if a CCD-based Raman system does not pass this noise test, then the additional source of noise (beyond fixed structure noise) must be identified and removed by experimental means. The main principles of the noise test are described below and illustrated in Fig. S5.

- We start from a large number of spectra, say $N_s = 5000$, and split them into two groups of $N_s/2 = 2500$ spectra. The spectra belonging to a specific group are chosen at random. We then take the difference between the average of each group to obtain a noise spectrum (where the fixed-structure noise has, by construction, been removed). The relative rms noise in the difference spectrum ϵ_{diff} is computed, from which the relative noise in the original average spectrum is deduced as $\epsilon(N_s/2) = \epsilon_{\mathrm{diff}}\sqrt{2}$. In practice, this step is repeated 100 times (with different random permutations) and the resulting $\epsilon(N_s/2)$ averaged over these 100 trials.
- We then repeat the whole process, but picking two groups of $N_s/4 = 1125$ (again with 100 iterations) to deduce $\epsilon(N_s/4)$, and then $N_s/8$, etc, with increasingly small numbers of spectra per group.
- The resulting dependence of ϵ (excluding fixed-structure noise) on N_s can then be plotted as in Fig. S5, and the expected $1/\sqrt{N_s}$ dependence asserted. The corresponding value for the entire collection of spectra $\epsilon(N_s = 5000)$ can also be obtained by extrapolation (it is of the order of $\epsilon(N_s/2 = 2500)\sqrt{2}$ if the expected $1/\sqrt{N_s}$ dependence is observed).
- The experimentally determined value of $\epsilon(N_s = 5000)$ can then be compared to the theoretical value for a photon-noise limited spectrum $\epsilon_{\mathrm{Theo}} = 1/\sqrt{N}$, where N is the total number of collected photons, which can be calculated if the CCD gain G is known. Alternatively, the fit can be used to measure the actual CCD gain, assuming that the spectra are photon-noise limited. A measured gain of $G = 15.2\,\mathrm{photons/cts}$ was inferred for our CCD and used throughout this study. Note that CCD gains are instrument-dependent and typically differ slightly from their nominal value (which is 13.3 for our Symphony CCD).

If the $1/\sqrt{N_s}$-dependence is not observed or the experimental and theoretical values of the relative noise (or CCD gain) do not match, then it indicates that something is wrong, and the PD-RRS method is unlikely to work at its best. A potential source of failure of these tests is, for example, *saturation* corresponding to reaching the full-well capacity of the well used for collecting the charges of a column of the CCD array. This is different to electronic saturation, which caps the signal level, and is therefore much less obvious to spot. The signal is not apparently saturating as seen by simple inspection of the spectrum, but it is saturating in the reading process. Even before full saturation occurs, non-linearity may arise in the response of the CCD, and tests like the one discussed in this section might fail. The bottom line is that these experiments require a full understanding of the technical details of the CCD being used (dynamic range, full-well capacity, linearity, etc). Without a full understanding of the technical characteristics, it is likely that one detail might fail, and the test for a shot-noise limited signal might not be successful.

Finally, even if the tests discussed above are passed, there are still instances where the measured PD-RRS noise is larger than what it is expected; $\epsilon_{\mathrm{PDRRS}} > \epsilon_{\mathrm{Ph}}\sqrt{2}$. This indicates that other sources of noise contribute to the PD-RRS spectrum. In all our measurements, this could always be tracked down to the presence of residual Fabry-Perot-like oscillations or interferences. As discussed earlier, this can be removed if needed with a careful design of the experimental setup, and some basic precautions.

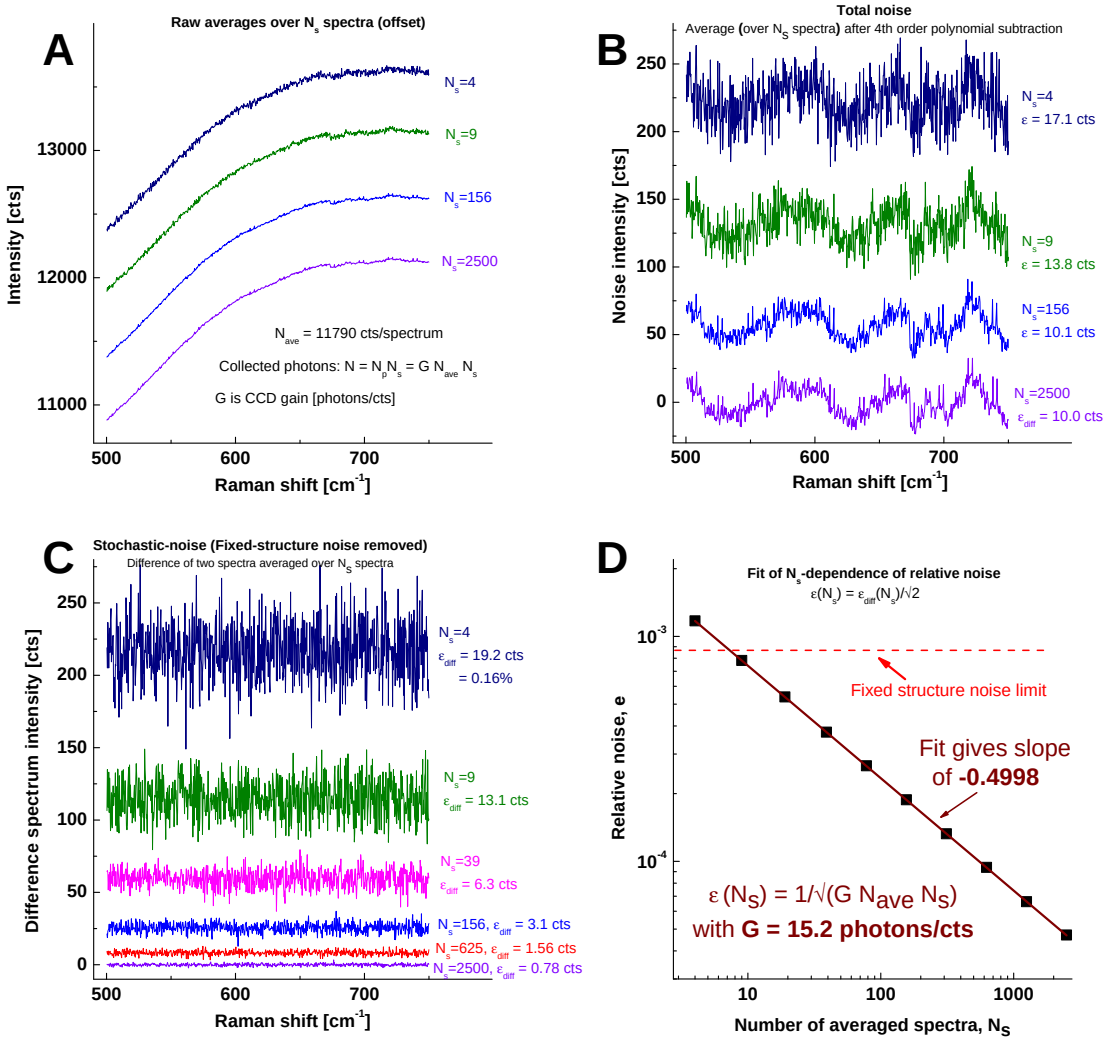

FIG. S5: Example of CCD-noise test for our system. A total of $N_s = 5000$ spectra with fixed integration time are taken for the signal of NB excited at 647 nm (the exact nature of the signal is irrelevant for this test). In **A** we show the result of averaging the signal over a number N_s =4, 9, 156 and 2500, of (randomly selected) spectra. After subtraction of a 4th-order polynomial from each, we obtain the results in **B**, where we can observe the gradual reduction of the true stochastic noise (dominated by photon noise) and the simultaneous emergence of the fixed structure noise with increasing number of spectra averaging. In fact, for $N_s > 10 - 100$, we can observe that the relative noise ϵ hardly changes, and is completely dominated by fixed structures in the spectra. In **C** we take differences of two spectra averaged over N_s randomly chosen spectra, for different values of N_s. This eliminates by definition the fixed structure noise (and any signal contained in the spectra in this case), and allows us to observe the true stochastic noise in the spectra. Now ϵ does decrease with N_s, as expected, and its variation is plotted in **D**. As can be appreciated from **D**, ϵ follows the expected scaling $\propto 1/\sqrt{N_s}$ (slope=-0.5). The dashed red line in **D** represents the limit imposed by the fixed structure noise found in **B**. It is quite clear that only the removal of fixed structure noise can achieve the level of $\epsilon \sim 10^{-4}$ needed to observe RR signals above the fluorescence background.

S.V. SOME DEFINITIONS OF RELEVANT CROSS-SECTIONS

In the following and in the main text, Raman cross-sections are characterized by the 90°-scattering differential Raman cross-section (spectrally integrated over the Raman peak and all outgoing polarizations), denoted $d\sigma^R_\Omega \equiv d\sigma^R/d\Omega$, typically expressed in units of [cm^2/sr]. We note that the total Raman cross-section σ^R is also sometimes used instead [1, 2], and can be easily deduced from [3]:

$$\sigma^R = \frac{8\pi}{3}\frac{1+2\rho_R}{1+\rho_R}d\sigma^R_\Omega, \tag{S1}$$

where ρ_R is the Raman depolarization ratio.

Because we are interested in quantifying the fluorescence intensity under the Raman peak (as opposed to the total intensity), we will also use the 90°-scattering

doubly-differential fluorescence cross-section, denoted $d\sigma^F_{\Omega\bar{\nu}} \equiv d^2\sigma^F/(d\Omega d\bar{\nu})$, which we will express in units of $[\mathrm{cm}^2/\mathrm{sr}/\mathrm{cm}^{-1} \equiv \mathrm{cm}^3/\mathrm{sr}]$. Note that it is not spectrally integrated and therefore depends on the spectral position (wavelength) at which it is evaluated (and also obviously on the excitation wavelength). This is necessary because the fluorescence has a very different spectral width from a typical Raman peak. Accordingly, we are only interested in quantifying the fluorescence over a much smaller spectral range than its natural width; hence the need for doubly-differential fluorescence cross section. Note that the standard differential fluorescence cross-section $d\sigma^F_\Omega$ would be given by spectral integration as:

$$d\sigma^F_\Omega = \int d\sigma^F_{\Omega\bar{\nu}}(\bar{\nu}) d\bar{\nu}. \tag{S2}$$

From these basic cross-sections, one can in principle infer the ratio of Raman-to-fluorescence intensity, and therefore how difficult a RR measurements will be (or more quantitatively: which relative noise level ϵ is required for a direct RR measurement or a PD-RRS experiment). For this, we however need to know the Raman peak intensity (rather than the integrated intensity) and this is also characterized a doubly-differential (Raman) cross-section, $d\sigma^R_{\Omega\bar{\nu}}$. The latter depends on the linewidth (and to a lesser degree the lineshape) of the Raman peak. For a Lorentzian lineshape with Full Width at Half Maximum (FWHM) Γ, it is straightforward to show that the peak Raman intensity is:

$$d\sigma^R_{\Omega\bar{\nu}} = \frac{2}{\pi\Gamma} d\sigma^R_\Omega. \tag{S3}$$

We can therefore define, for a given Raman peak and excitation wavelength, the Raman-to-fluorescence intensity ratio in the parallel polarization configuration, $R^\parallel$ [adimensional] as:

$$R^\parallel = \frac{d\sigma^{R-\parallel}_{\Omega\bar{\nu}}}{d\sigma^{F-\parallel}_{\Omega\bar{\nu}}} = \frac{2\, d\sigma^R_\Omega}{\pi\Gamma(1+\rho_R)\, d\sigma^{F-\parallel}_{\Omega\bar{\nu}}}, \tag{S4}$$

which provides a measure of how difficult it is to directly measure the Raman signal on top of the fluorescence background (the lower $R^\parallel$, the harder it is).

In a PD-RRS experiment, we are not directly measuring $R^\parallel$, but the difference between the $\parallel$ and $\perp$ spectra (with integration times adjusted to $1/\rho_F$ times longer in the latter case to match the fluorescence backgrounds). The relative amplitude of the PD-RRS peak Raman intensity is therefore:

$$R^{\mathrm{PDRRS}} = (1-\rho_R/\rho_F)R^\parallel = \frac{2}{\pi\Gamma}\frac{1-\rho_R/\rho_F}{1+\rho_R}\frac{d\sigma^R_\Omega}{d\sigma^{F-\parallel}_{\Omega\bar{\nu}}}. \tag{S5}$$

This figure provides an estimate of how difficult it is to measure the RR peak above the background in PD-RRS. For a typical PD-RRS measurement to resolve the Raman peak above the noise, one will typically need a relative noise level of $\epsilon_{\mathrm{PDRRS}} \leq R^{\mathrm{PDRRS}}/2$.

Examples of experimentally determined values for the parameters defined in this section are given in Tab. S.I.

S.VI. EXPERIMENTAL DETERMINATION OF RESONANCE RAMAN CROSS-SECTIONS

One issue that arises in the calculation of the absolute differential cross section from the integrated intensity of the Raman peaks is to find a proper reference to normalize it to. One possibility is to use a substance of known differential cross section in the same scattering configuration and cell that is used for the resonance Raman measurement. An example of the latter is the use of 2-bromo-2-methyl-propane (2B2MP), which has been extensively characterized experimentally and theoretically (see the supplementary information in Ref. [4]). There are, however, some potential problems with this approach too, for the scattering volume in 2B2MP (which is transparent) is *not* the same as the scattering volume in the cell with the dye, due to absorption effects. As a matter of fact, absorption effects can be significant under resonance conditions, even for moderate concentrations of the order of a few μM. In addition, photobleaching of the dye might add additional complications to estimate the effective concentration producing the signal. For all these reasons, we developed a normalization technique that steers away from these problems, and it is based on a two-step measurement as follows:

- The fluorescence cross section, $d\sigma^{F-\parallel}_{\Omega\bar{\nu}}$ is first characterized in the parallel polarization configuration. This is done by performing a fluorescence measurement at relatively low concentration (less than $\sim 1\,\mu$M where absorption effects are negligible), and low laser power (where photobleaching is negligible, as checked by linearity tests). In that manner, we can basically avoid the adverse effects of both absorption and photobleaching. We use 2B2MP as a cross-section standard; its $516\,\mathrm{cm}^{-1}$ Raman peak has a depolarization ratio of 0.16 and a differential Raman cross-section of $d\sigma^R_\Omega = 5.4\times10^{-30}\,\mathrm{cm}^2/\mathrm{sr}$ at 633 nm [4]). The latter is appropriately scaled by the ω^4-dependence of the cross section for other excitation wavelengths (no resonance Raman enhancement are expected because the absorption of 2B2MP is deep in the UV). We focus in particular on the fluorescence intensity at the spectral position of the Raman peak under study, and by comparison with 2B2MP we can deduce the doubly-differential fluorescence cross-section for parallel polarization: $d\sigma^{F-\parallel}_{\Omega\bar{\nu}}$. During this preliminary experiment, we also measure the fluorescence depolarization ratio (at the Raman peak position): $\rho_F = d\sigma^{F-\perp}_{\Omega\bar{\nu}}/d\sigma^{F-\parallel}_{\Omega\bar{\nu}}$, which is needed for the analysis of the PD-RRS data. Examples of experimentally determined values are given in Tab. S.I.

- The actual measurement of the RR cross sections can then be done at higher dye concentrations ($\sim\mu$M) trying to maximize the number of photons collected per unit time. This can be done even if

the scattering volume is not exactly the same as 2B2MP and/or there are effects from photobleaching. The basic idea is that the same dye molecules that are producing the fluorescence are also producing the Raman signal. The fluorescence background under the Raman peak (with a known independently measured cross-section) can then serve as reference cross-section to determine the measured differential cross-section of the PD-RRS Raman peak: $d\sigma_{\Omega}^{\mathrm{PDRRS}}$. From here, the actual RR cross-section $d\sigma_{\Omega}^{R}$ can be inferred from the PD-RRS measurement, as explained in the main text (see Eq. 1).

The main advantage of this two-step approach is that it is self-normalizing with respect to dye concentration, laser absorption, and photo-bleaching. These potential problems only need to be taken care of in the much easier preliminary measurement of the fluorescence cross-section.

S.VII. ERROR ESTIMATION

The main sources or errors in these experiments come from three origins:

- Reproducibility errors with exact dye concentrations. This can be more noticeable at low concentrations, where we have observed some wall-absorption effects of dyes on the optical cells. Overall, we strove to minimize these errors by repeating measurements several times and checking the exact concentration before each measurement with an absorption spectrum. This latter measure is strongly recommended for these experiments and tend to minimize any inaccuracy in dilution effects, or any of its associated wall absorption phenomena.

- Reproducibility effects in the optical alignment of the reference cells. When comparing the measured doubly-differential fluorescence cross section with the 2B2MP reference, two measurements with two different cells are necessary. Special care is required to ensure that the optical alignment of the two cells is equivalent; and that reproducible values are obtained in the process of removing and aligning the cells repeatedly. In our experiments, we obtained a reproducibility within $\sim 5\%$ for successive measurements of the reference sample.

- The errors arising from the fit of the Raman peak in the PD-RRS spectrum are dominated by uncertainties in the linewidth and lineshape. The chosen peak shape to fit the Raman signal has a slight influence on the value of the reported cross section. For example, if instead of choosing a Lorentzian one chooses a Gaussian peak shape, it is possible to obtain a satisfactory fit corresponding to a slightly smaller cross-section. This comes from the fact that Loretzian and Gaussian peak shapes give slightly different weights to the "wings" of the peak above the background. Similarly, despite the relatively high-resolution gratings used in these experiments, a change of $\sim 10\%$ in the FWHM does not significantly affect the quality of the fit. Because the integrated intensity is proportional to the FWHM, it results in a similar uncertainty in the cross-section. Accordingly, uncertainties in lineshape and linewidth result in an estimated uncertainty of $\sim 15-20\%$ for the Raman cross-section, which we believe to be the dominant source of errors in our reported values. Formally, the reported cross sections should include a specification of the peak shape used to obtain it. All our reported values are for Lorentzian peak shapes.

Overall, having repeated the experiments several times to gain a feeling for their reproducibility under slightly different experimental conditions of alignment, we estimate the accuracy of our experimental values to be within $\sim 20\%$, taking into account all the possible combined sources of errors.

S.VIII. SUPPLEMENTARY DATA

In this final section, we provide a supplementary table S.I with a summary of the main quantities measured and supplementary figures with full details of the PD-RRS measurements carried out in this work: rhodamine 6G in water resonantly excited at 514 nm (Fig. S6) and Nile blue at 633 nm in both ethanol (Fig. S7) and water (Fig. S8).

TABLE S.I: Summary of the experimental values obtained for the most important quantities investigated in this work, and defined in this supplementary online material. Note that † indicates a large uncertainty because of small fluorescence signals and the Raman depolarization ratios of 1/3 are assumed on the basis of standard RR theory [5], as discussed in the text.

	NB/Water $\Delta\bar{\nu}_R = 595\,\mathrm{cm}^{-1}$					NB/Ethanol $594\,\mathrm{cm}^{-1}$	R6G/water $612\,\mathrm{cm}^{-1}$
λ_L [nm]	514.5	531	568	633	647	633	514.5
σ^{Abs} [cm^2]	1.7×10^{-17}	2.9×10^{-17}	9.2×10^{-17}	2.5×10^{-16}	2.3×10^{-16}	2.6×10^{-16}	2.6×10^{-16}
$d\sigma^{F-\parallel}_{\Omega\bar{\nu}}(\Delta\bar{\nu}_R)$ [$\mathrm{cm}^2/\mathrm{sr}/\mathrm{cm}^{-1}$]	3.2×10^{-27}†	8.8×10^{-27}†	5.7×10^{-26}	1.8×10^{-22}	2.4×10^{-22}	1.7×10^{-21}	1.2×10^{-21}
ρ_F	0.72†	0.71†	0.86	0.76	0.80	0.88	0.95
QY	-	-	-	4%	4%	25%	95%
$d\sigma^R_\Omega$ [$\mathrm{cm}^2/\mathrm{sr}$]	5.0×10^{-26}	9.5×10^{-26}	3.8×10^{-25}	3.0×10^{-24}	2.2×10^{-24}	4.7×10^{-24}	1.9×10^{-24}
ρ_R	0.41	0.41	0.35	1/3	1/3	1/3	1/3
Γ [cm^{-1}]	7.6	6.8	6.5	7.7	7.5	4.1	5.6
σ^R [cm^2]	5.4×10^{-25}	1.0×10^{-24}	4.0×10^{-24}	3.1×10^{-23}	2.3×10^{-23}	4.9×10^{-23}	2.0×10^{-23}
$R^{\parallel}$	0.9†	0.72†	0.48	1.0×10^{-3}	5.8×10^{-4}	3.2×10^{-4}	1.3×10^{-4}
$R^{\mathrm{PD-RRS}}$	0.4†	0.3†	0.29	5.8×10^{-4}	3.3×10^{-4}	2.0×10^{-4}	8.8×10^{-5}

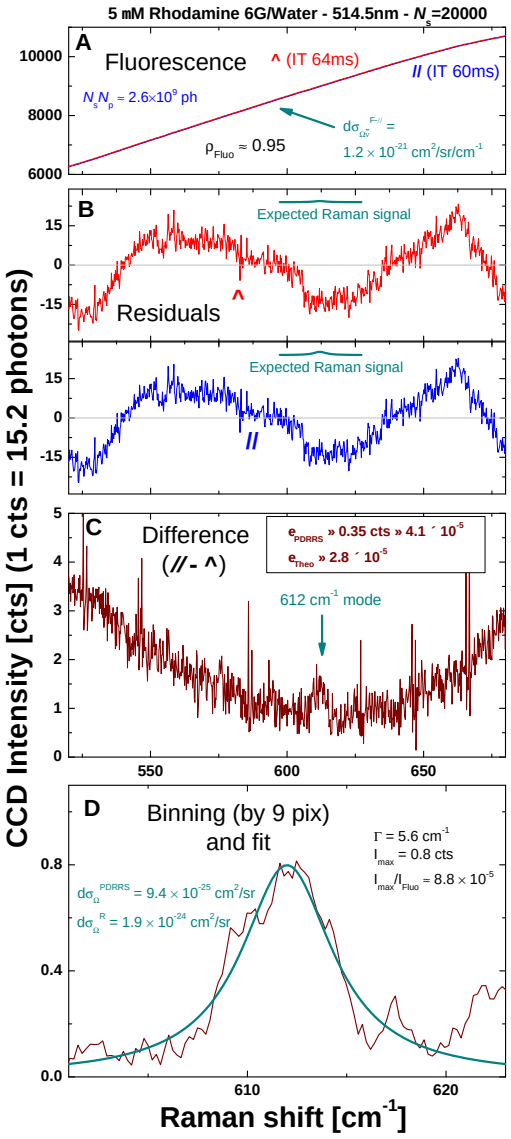

FIG. S6: PD-RRS measurement for the 612 cm^{-1} mode of Rhodamine 6G in water at 514 nm excitation using $N_s = 2 \times 10^4$ spectra for each polarization. (**A**) Fluorescence spectra for each polarization, note the different integration time (IT) to account for the fluorescence depolarization ratio $\rho_F \approx 0.95$. (**B**) Residuals of **A** after 4th-order polynomial subtraction, showing an almost identical fixed-structure noise. The intensities of the expected Raman peaks (computed *a posteriori*) are indicated as a guide. (**C**) PD-RRS spectrum obtained from subtraction of the $\parallel$ and $\perp$ configuration average spectra, where the Raman peak is clearly visible. Note that the PD-RRS spectrum is here not photon-noise-limited (additional noise is visible, but does not prevent the observation of the Raman peak). (**D**) PD-RRS spectrum (binned by 9 pixels) in the Raman peak region and Lorentzian fit to the peak. Note that thanks to the relatively high dispersion grating used in this experiment (the wavenumber spacing between consecutive pixel is 0.2 cm^{-1}), we can improve further the noise level by binning the spectrum by 9 consecutive pixels.

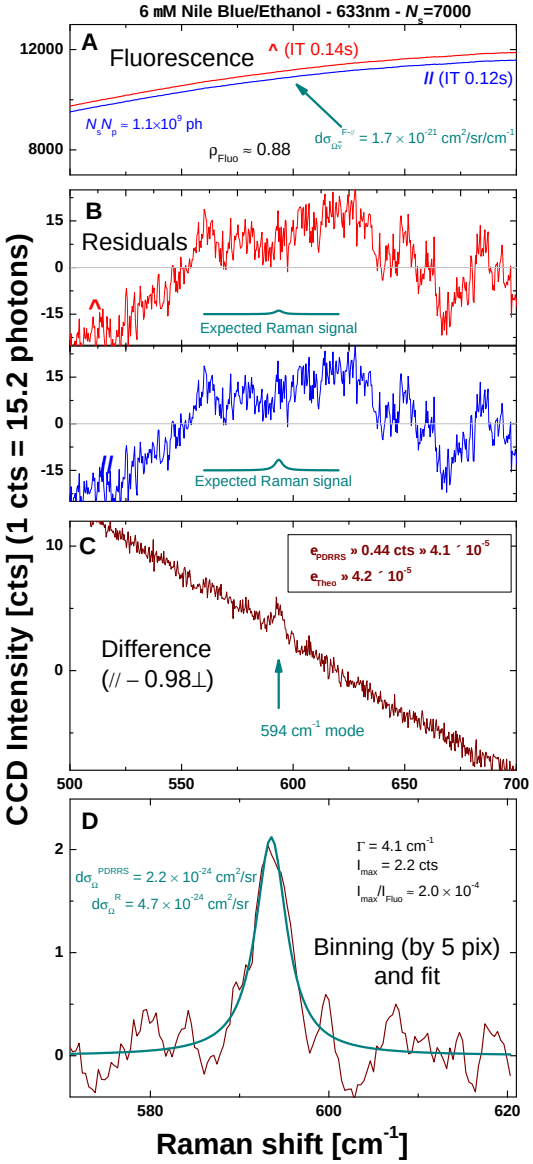

FIG. S7: PD-RRS measurement for the 594 cm^{-1} mode of Nile Blue in ethanol at 633 nm excitation using $N_s = 7000$ spectra for each polarization. (**A**) Fluorescence spectra for each polarization, note the different integration time (IT) to account for the fluorescence depolarization ratio $\rho_F \approx 0.88$. (**B**) Residuals of **A** after 4th-order polynomial subtraction, showing an almost identical fixed-structure noise. The intensities of the expected Raman peaks (computed *a posteriori*) are indicated as a guide. (**C**) PD-RRS spectrum obtained from subtraction of the ∥ and ⊥ configuration average spectra, where the Raman peak is clearly visible. (**D**) PD-RRS spectrum (binned by 5 pixels) in the Raman peak region and Lorentzian fit to the peak. Note that thanks to the relatively high dispersion grating used in this experiment (the wavenumber spacing between consecutive pixel is 0.36 cm^{-1}), we can improve further the noise level by binning the spectrum by 5 consecutive pixels.

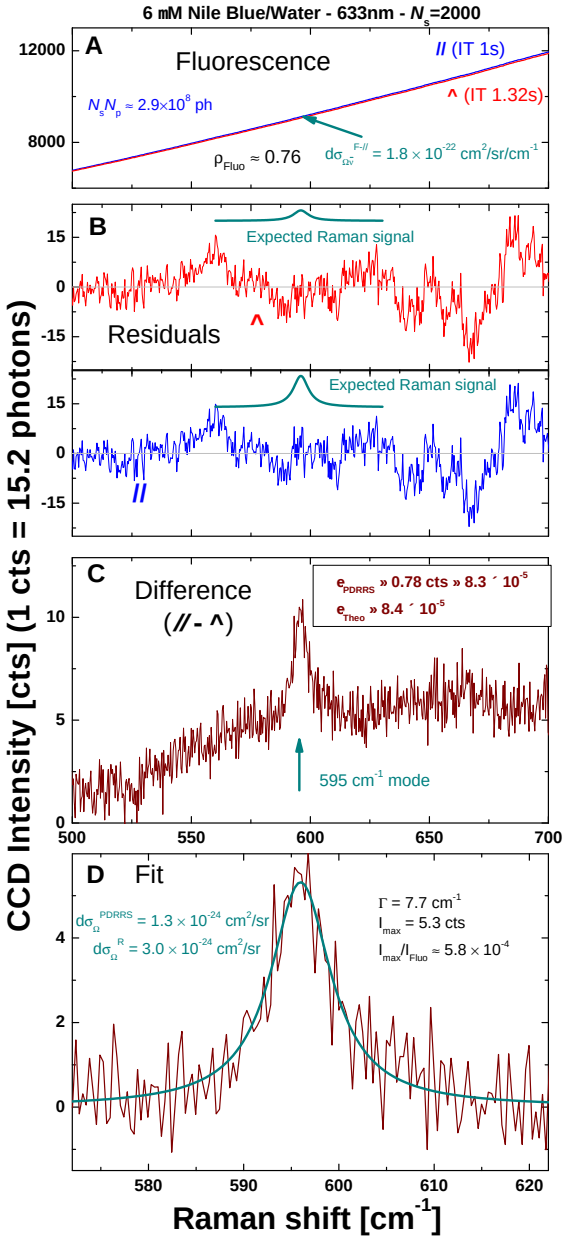

FIG. S8: PD-RRS measurement for the 595 cm^{-1} mode of Nile Blue in water at 633 nm excitation using $N_s = 2000$ spectra for each polarization. (**A**) Fluorescence spectra for each polarization, note the different integration time (IT) to account for the fluorescence depolarization ratio $\rho_F \approx 0.76$. (**B**) Residuals of **A** after 4th-order polynomial subtraction, showing an almost identical fixed-structure noise. The intensities of the expected Raman peaks (computed *a posteriori*) are indicated as a guide. (**C**) PD-RRS spectrum obtained from subtraction of the $\parallel$ and $\perp$ configuration average spectra, where the Raman peak is clearly visible. (**D**) PD-RRS spectrum in the Raman peak region and Lorentzian fit to the peak.

[1] Lawless, M. K.; ; Mathies, R. A. *J. Chem. Phys.* **1992**, *96*, 8037–8045.
[2] Shim, S.; Stuart, C. M.; Mathies, R. A. *ChemPhysChem* **2008**, *9*, 697–699.
[3] Le Ru, E. C.; Etchegoin, P. G. *Principles of Surface Enhanced Raman Spectroscopy and Related Plasmonic Effects*; Elsevier: Amsterdam, 2009.
[4] Le Ru, E. C.; Blackie, E.; Meyer, M.; Etchegoin, P. G. *J. Phys. Chem. C* **2007**, *111*, 13794–13803.
[5] Clark, R. J. H.; Dines, T. J. *Angew. Chem. Int. Ed.* **1986**, *25*, 131–158.